Journal of Energy Chemistry 114 (2026) 799–807

Contents lists available at ScienceDirect

Journal of Energy Chemistry

journal homepage: www.elsevier.com/locate/jechem

http://www.journals.elsevier.com/journal-of-energy-chemistry/

Flame retardant polymer current collector for safer and higher energy density lithium-metal batteries

Mintao Wan [a,b,1], Huifang Fei [c,1], Haowen Liu [d,e], Nae-Lih Wu [d,e], Stefano Passerini [a,b,f,*], Dominic Bresser [a,b,g,*]

[a] Helmholtz Institute Ulm (HIU), Ulm 89081, Germany
[b] Karlsruhe Institute of Technology (KIT), Karlsruhe 76021, Germany
[c] College of Materials Science and Engineering, Nanjing Tech University, Nanjing 211816, Jiangsu, China
[d] Department of Chemical Engineering, Taiwan University, Taipei 10617, Taiwan, China
[e] Advanced Research Center for Green Materials Science and Technology, Taiwan University, Taipei 10617, Taiwan, China
[f] Austrian Institute of Technology (AIT), Center for Transport Technologies, 1210 Wien, Austria
[g] Ulm University (UUlm), Ulm 89069, Germany

ARTICLE INFO

Article history:
Received 19 August 2025
Revised 19 October 2025
Accepted 26 October 2025
Available online 10 November 2025

Keywords:
Current collector
Polymer
Flame retardant
Lithium-metal anode
Battery

ABSTRACT

Energy density and safety are two crucial parameters when evaluating lithium-metal batteries (LMBs). Herein, we present an ultralight polymer-based current collector, incorporating flame-retardant materials, designed specifically for thin lithium-metal anodes. Compared to the traditional copper current collector (8.96 mg cm^{-2}, 10 μm thick), the polymer-based current collector (12 μm thick) has a significantly lower areal density of 1.41 mg cm^{-2}, i.e., only one-sixth of the copper collector, thus enabling substantially higher energy densities. Accordingly, when employed in Li||NMC_{622} full-cells, the polymer-based current collector enables a specific energy of 449 Wh kg^{-1}, representing a notable improvement of about 14.5% compared to cells employing a classic copper current collector. The inclusion of $Al(OH)_3$ as a flame retardant into the current collector suppresses flammability and, thereby, significantly improves the safety of the resulting LMBs.

1. Introduction

Energy density and safety are two crucial properties for batteries for electric vehicles [1–3]. Lithium-metal batteries (LMBs), utilizing lithium metal as the negative electrode, possess potentially a substantially higher energy density compared to state-of-the-art lithium-ion batteries due to the high specific capacity (~3860 mAh g^{-1}) and low operating voltage (−3.04 V vs. the standard hydrogen electrode) of metallic lithium [4,5]. However, the eventual energy density of LMBs heavily depends on the thickness of the lithium-metal anode. In fact, to achieve cell-level specific energies well exceeding that of lithium-ion batteries, it is necessary to use rather thin lithium-metal anodes in the range of a few tens of micrometers [6–9]. Despite numerous ongoing research endeavors to tackle the challenges of lithium-metal anodes, including dendrite formation, safety issues, and the high reactivity with the electrolyte [10–14], a commonly overlooked issue is the electron transport within a bare, thin lithium-metal foil (not to mention the related challenges for the handling and processing). In fact, the thinner the lithium-metal foil, the greater the likelihood of encountering issues such as poor electron transport within the lithium foil due to cracks arising from an uneven stripping/plating process [15]. The use of an electrochemically inert metal foil, such as copper represents a straightforward and very simple to implement approach to overcome these challenges [16,17]. However, copper is relatively heavy owing to its high density of 8.96 g cm^{-3}, and the combination of, for instance, a 10 μm thick copper foil with a 50 μm thick lithium foil would mean that more than 77% of the total mass stems from the inactive copper current collector. As a result, the achievable specific energy at cell level remains highly limited [18,19]. Recently, some of the literature reported the introduction of polymer- or carbon-based materials in the-energy storage systems to reduce the overall weight of the whole system, thus increasing the energy density [20,21]. We have also reported a much lighter alternative based on a composite

* Corresponding authors.
E-mail addresses: stefano.passerini@kit.edu (S. Passerini), dominic.bresser@kit.edu (D. Bresser).
[1] These authors contributed equally to this work.

https://doi.org/10.1016/j.jechem.2025.10.052

of polyethylene (PE) and conductive carbon (C) in our last work [22]. While this allowed for a substantially higher specific energy and extended cycle life compared to neat lithium foil and the commonly used copper current collector, this PE/C composite apparently comes along with a higher flammability compared to classically used copper foil, which renders such system advantageous from the performance perspective, but at the expense of a somewhat decreased safety.

Herein, we address this issue by introducing $Al(OH)_3$ as flame retardant into the PE/C current collector, targeting an enhanced safety while maintaining the advantageous electrochemical behavior and the energy density gain of the lightweight PE/C current collector reported earlier. The resulting 12 μm thick PE/C/$Al(OH)_3$ membranes have a mass of only 1.41 mg cm^{-2}, which is 1/6 of a 10 μm thick Cu current collector, thus, providing a specific energy increase of about 15% in Li||NMC_{622} full-cells compared to cells employing a copper current collector. Simultaneously, the introduction of ($Al(OH)_3$) into the current collector renders such system essentially non-flammable, while, indeed, advantageously not affecting the charge storage and transport reactions in the cell upon cycling.

2. Experimental

2.1. Preparation of the PE/C/$Al(OH)_3$ current collector

Firstly, polyethylene (PE) powder, carbon black (C), and 0 wt.%, 20 wt.%, or 40 wt.% of $Al(OH)_3$ were mixed *via* ball milling at 400 rotations min^{-1} for 4 h (the PE:C ratio was 7:3). The resulting mixtures were pressed under a gradually increasing pressure of up to 200 t at a temperature of 120 °C. Finally, the thickness of the three polymer membranes was adjusted to 12 μm by hot calendaring at 120 ℃.

2.2. Basic characterization

The morphology and composition of the PE/C/$Al(OH)_3$ polymer membranes were analyzed by means of FT-IR spectroscopy (Fourier-transform infrared spectroscopy, Bruker VERTEX), SEM (scanning electron microscope, ZEISS Crossbeam 340), and XRD (X-ray diffraction, Bruker D8 with Cu K_α radiation). The conductivity of the current collectors was measured using a Jandel CYL-RM3000 Four Point Probe System. Tensile strength measurements were conducted using dynamic mechanical analysis (DMA, Q800, TA Instruments, Inc.) *via* an isotactic force test with a force ramp rate of 1 N min^{-1} at 25 ℃ until a maximum of 18 N was reached or until the sample broke. Flammability tests were performed on polymer membranes with a size of 0.5 × 3 cm^2. DSC (differential scanning calorimetry) measurements were performed on a TA Instruments Q2000 in a temperature range from 20 ℃ to 400 ℃ with a heating rate of 5 ℃ min^{-1} under N_2 atmosphere. For the ex situ SEM and XPS (X-ray photoelectron spectroscopy) characterization, the cycled Cu and PE/C/$Al(OH)_3$ current collectors were recovered by disassembling the cycled Li||Cu and Li||PE/C/$Al(OH)_3$ coin cells in an argon-filed glovebox (MBraun, O_2 and H_2O content of less than 0.1 ppm). XPS was conducted on a PHI 5800 Multi Technique ESCA system (Physical Electronics) using monochromatic Al K_α radiation (300 W), and a detection angle of 45. The samples were neutralized with electrons from a flood gun (current 3 μA) to compensate for charging effects at the surface. For the binding energy calibration, the C 1*s* peak was set to 284.8 eV. After cell disassembly, the cycled electrodes were washed with DMC (dimethyl carbonate) to remove any residual electrolyte and then transferred to the SEM or XPS using an airtight transfer box to prevent any contamination from the ambient atmosphere.

2.3. Electrochemical testing

2032 coin-type Li||Cu and Li||PE/C/$Al(OH)_3$ cells were assembled in an argon-filled glove box (MBraun, O_2 and H_2O content of less than 0.1 ppm). Cyclic voltammetry (CV) tests of Li||Cu and Li||PE/C cells were performed using a Biologic VMP system in the voltage range from −0.5 V to 1.0 V (vs. Li^+/Li), with a sweep rate of 10 mV s^{-1}. The Li||NMC_{622}, Li-Cu||NMC_{622}, and Li-PE/C/$Al(OH)_3$||NMC_{622} pouch cells were assembled in the dry room with a dew point of less than −70 ℃. The positive electrodes were composed of 90 wt.% of $LiNi_{0.6}Mn_{0.2}Co_{0.2}O_2$ (NMC_{622}, BASF) as the active material, 5 wt.% polyvinylidene fluoride (PVdF, Solef 6020), and 5 wt.% carbon black (Super C65, IMERYS). The electrodes for the constant current cycling and rate capability tests had an active material mass loading of 25 and 6.5 mg cm^{-2}, respectively. The lithium foil (Honjo) had a thickness of 50 μm, equivalent to ca. 10 mAh cm^{-2}. 1 M lithium hexafluorophosphate ($LiPF_6$, Sigma-Aldrich) dissolved in a 4:1 vol mixture of dimethyl carbonate (DMC, Sigma-Aldrich) and fluoroethylene carbonate (FEC, Sigma-Aldrich) served as the electrolyte, and Celgard 2500 sheets as the separator. For the constant current cycling, the cut-off voltages were set to 2.8 and 4.4 V, and the charge and discharge were conducted at 0.3C and 0.5C, respectively (1C = 180 mA g^{-1}). For the evaluation of the rate capability, the cells were subjected to varying C rates of 0.5C, 1C, 2C, and 5C. Both tests were conducted at 20 ± 1 ℃ using a Maccor 4000 battery test equipment.

3. Results and discussion

3.1. Fabrication and basic characterization

PE and C (with a weight ratio of 7:3) plus varying amounts of $Al(OH)_3$ (0%, 20%, and 40%) were intimately mixed *via* ball milling. The resulting powders were hot pressed at 120 ℃, yielding a thin and flexible polymer film. Subsequently, the thickness of the polymer membrane was adjusted by hot calendaring (Fig. S1). This fabrication method is generally very simple and appears easily scalable, and the introduction of the flame retardant into the current collector provides the advantage that it does not affect any reaction inside the cell until it is really needed, which is different from its introduction into the electrolyte [23–26], where it frequently results in an increased viscosity and, thus, lower ionic conductivity, or into the separator [27,28], leading to a significantly greater thickness, or into the electrodes [29,30], where it potentially affects the interphase formation and/or the redox reactions occurring upon dis−/charge. The purely physical mixing of PE, C, and $Al(OH)_3$ was confirmed by Fourier transform infrared (FT-IR) spectroscopy, revealing that the incorporation of $Al(OH)_3$ had no effect on the absorption peaks of PE, which are located at 2921, 2850, 1463, and 729 cm^{-1}, representing the –C–$(C–H)_n$–C– ($n \geq 4$), –C–$(C–H)_n$–C– ($n \leq 3$), C–H and C–H function group, respectively (Fig. 1a). This was further confirmed by conducting X-ray diffraction (XRD) on a PE/C membrane, the $Al(OH)_3$ powder, and the PE/C/$Al(OH)_3$ membrane, showing that the composite is a simple physical mixture of the three components (Fig. 1b). Scanning electron microscopy (SEM) and energy dispersive X-ray (EDX) spectroscopy performed on the PE/C/$Al(OH)_3$ membranes indicated that both C and $Al(OH)_3$ were evenly distributed in the PE matrix (Fig. 1c). The thickness of the PE/C/$Al(OH)_3$ film was approximately 12 μm, and appears constrained by the relatively large particle size of the $Al(OH)_3$ powder (Fig. 1d, Fig. S2). Subsequently, the application-relevant properties of the PE/C/$Al(OH)_3$ membranes for use as current collector, such as the electronic conductivity, mechanical strength, and electrochemical stability, were determined. The electronic conductivity was assessed *via* Four-

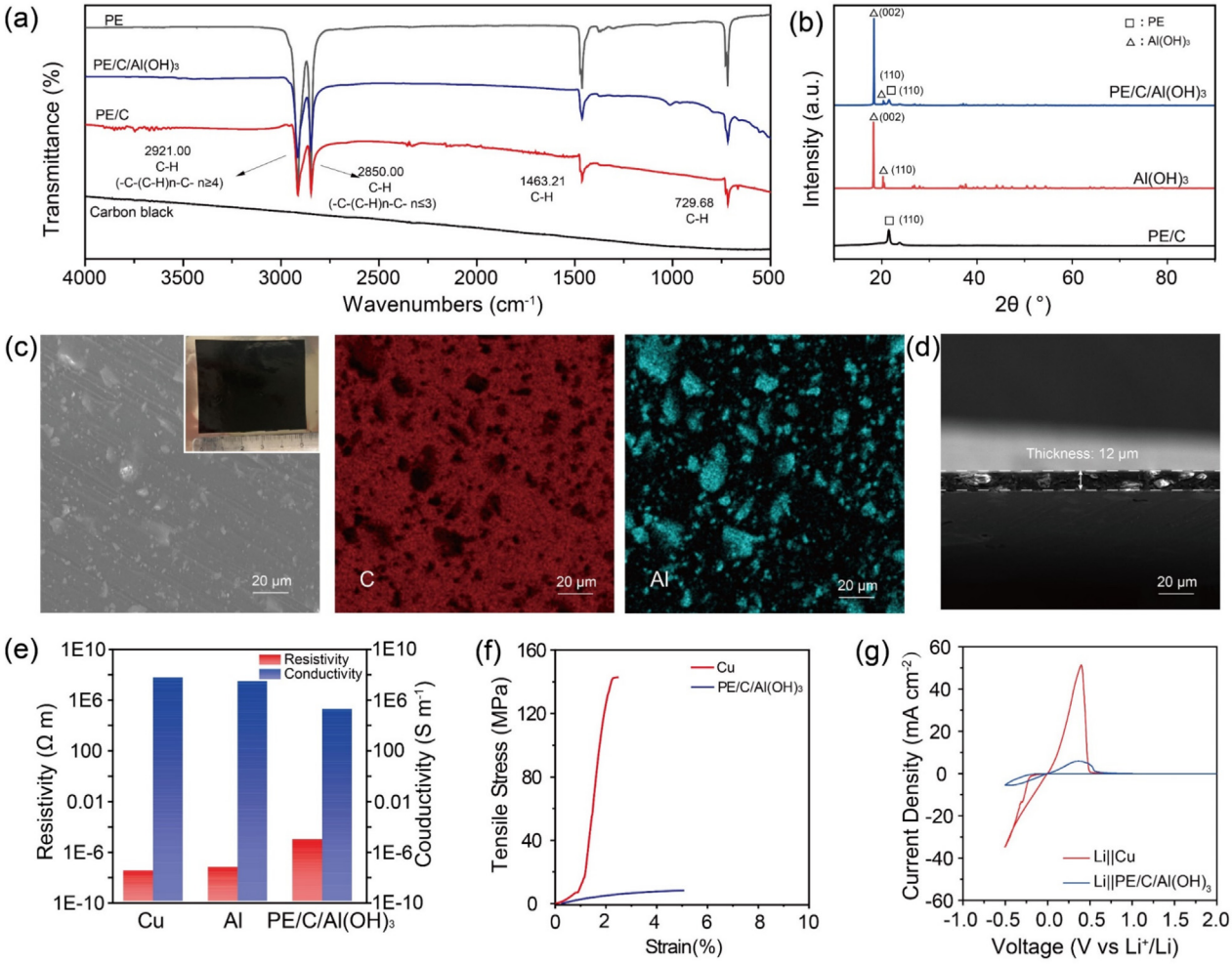

Fig. 1. Basic physicochemical, mechanical, and electrochemical characterization of the PE/C/Al(OH)$_3$ current collector. (a) FT-IR spectroscopy data of polyethylene, carbon black, the PE/C membrane, and the PE/C/Al(OH)$_3$ membrane. (b) X-ray diffraction pattern of the PE/C membrane, the Al(OH)$_3$ particles, and the PE/C/Al(OH)$_3$ membrane. (c) Top-view SEM micrograph of the PE/C/Al(OH)$_3$ membrane and the corresponding EDX mapping of C and Al. Inset in (c) is the photograph of the PE/C/Al(OH)$_3$ current collector. (d) Cross-sectional-view SEM micrograph of the PE/C/Al(OH)$_3$ membrane. (e) Electronic conductivity of Cu, Al, and the PE/C/Al(OH)$_3$ membrane. (f) Tensile strength of a 10 μm Cu foil and the 12 μm PE/C/Al(OH)$_3$ membrane. (g) Cyclic voltammetry results obtained for the Li||Cu cell and the Li||PE/C/Al(OH)$_3$ cell (sweep rate: 10 mV s^{-1}; reversing potentials: −0.5 and 1.0 V vs. Li$^+$/Li).

point probe measurements. Fig. 1(e) presents the conductivity test results of a commercial copper current collector, an aluminum current collector, and the PE/C/Al(OH)$_3$ membrane. The resistivity of the PE/C/Al(OH)$_3$ foil is 7.2×10^{-6} Ω m, which is about 100 times higher than the Cu current collector (2.46×10^{-8} Ω m) and the Al current collector (5.74×10^{-8} Ω m). However, not least in combination with metallic lithium on top, this conductivity should be more than sufficient for the application as current collector, as also later confirmed by the electrochemical studies. Fig. 1(f) presents the evaluation of the mechanical strength of the 10 μm Cu foil and 12 μm PE/C/Al(OH)$_3$ membranes. The tensile strength of the PE/C/Al(OH)$_3$ membrane is only ~5 MPa, i.e., much lower than the Cu (~145 MPa), but it withstands more than twice the strain as copper foil before breaking. The latter property, indicative of a high degree of flexibility, might be particularly advantageous in the case of lithium-metal anodes, which experience essentially infinite volume changes upon dis-/charge. Finally, cyclic voltammetry (CV) was carried out in a voltage range from −0.5 to 1.0 V (vs. Li$^+$/Li), i.e., in the working voltage range of the lithium-metal anode (Fig. 1g). The Li||PE/C/Al(OH)$_3$ cell showed essentially the same oxidation/reduction peaks as the Li||Cu cell, indicating that the same electrolyte degradation processes occur beside the lithium stripping and plating, and that the presence of Al(OH)$_3$ does not have any detectable effect. This is further corroborated by an ex situ XRD analysis of the PE/C/Al(OH)$_3$ membrane after 1 mA h cm^{-2} lithium plating, revealing the reflections of Al(OH)$_3$ and metallic lithium, suggesting that the Al(OH)$_3$ particles are well covered by PE, thus, preventing any chemical reaction between lithium and Al(OH)$_3$ (Fig. S3). Summarizing, the above results prove that there was no significant chemical reaction between the PE/C/Al(OH)$_3$ current collector and lithium or the electrolyte—at least nothing different from the classically used metallic copper—thus proving the general suitability and applicability of the PE/C/Al(OH)$_3$ membranes as current collector for LMBs.

In Fig. 2(a), the densities of bare lithium, copper, and PE/C/Al(OH)$_3$ are compared. Notably, the polymer-based PE/C/Al(OH)$_3$ foil has a mass density of only 1.17 g cm^{-3} due to its ultralight components, specifically, PE and C, resulting in an areal density of just 1.41 mg cm^{-2}. When the lightweight PE/C/Al(OH)$_3$ foil is combined with a thin lithium foil of 50 μm to form an electrode, the resulting Li-PE/C/Al(OH)$_3$ anode has a total areal density of only 4.08 mg cm^{-2} (Fig. 2b and Fig. S4). This value is only 1.5 times higher than that of a bare lithium-metal anode (2.67 mg cm^{-2}), but it is also only about one-third of the areal density of a Li-Cu electrode

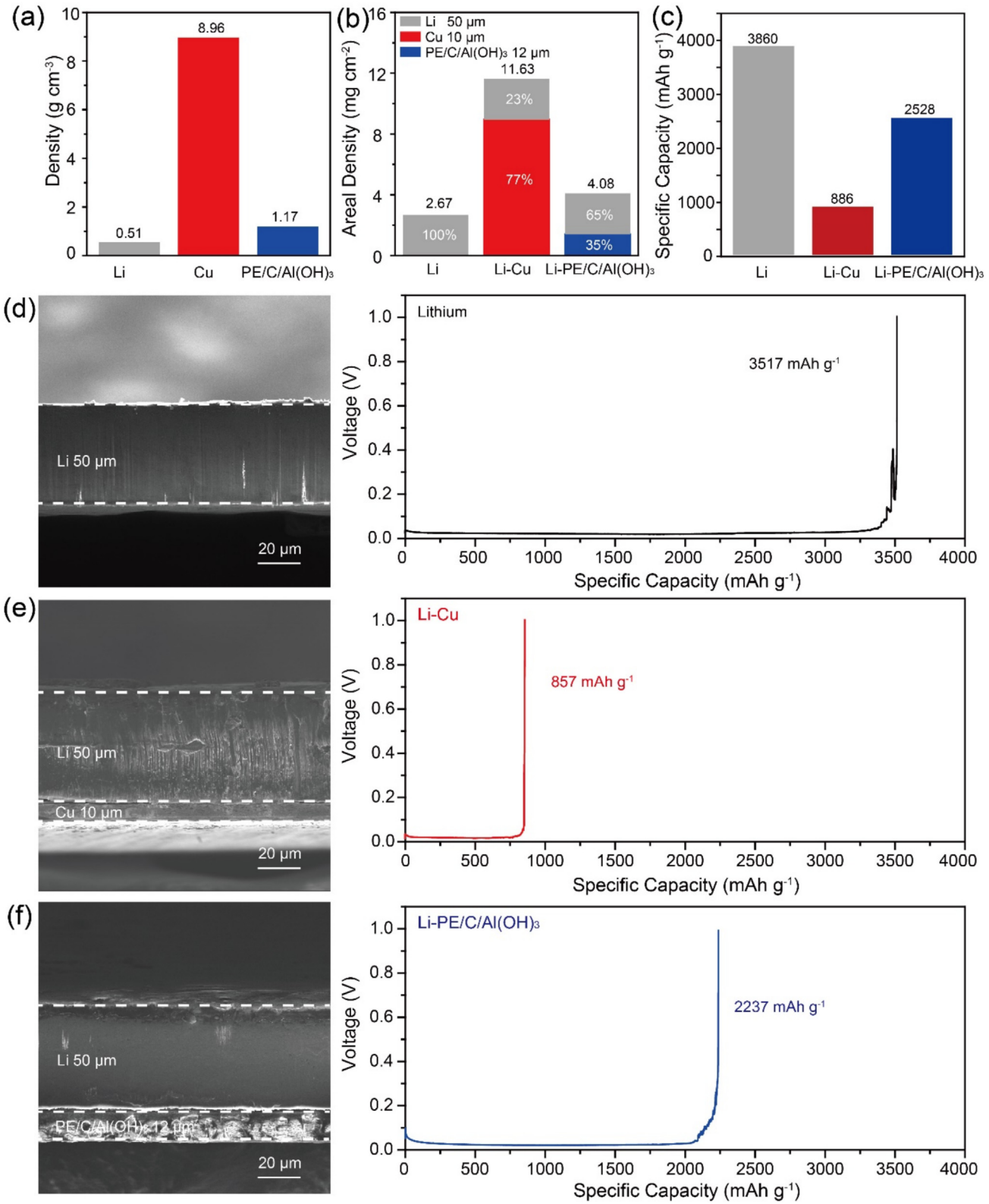

Fig. 2. Evaluation of the impact of the current collector on the overall specific capacity of the negative electrode. (a) Comparison of the density of neat lithium foil, copper foil, and the PE/C/Al(OH)$_3$ membrane. Comparison of the (b) areal density and (c) theoretical specific capacity of the neat lithium-metal anode, the Li-Cu anode, and the Li-PE/C/Al(OH)$_3$ anode (in all three cases for a lithium foil/layer with a thickness of 50 μm). Cross-sectional SEM micrographs (left) and the experimentally determined specific capacity (right) of (d) the neat lithium-metal anode, (e) the Li-Cu anode, and (f) the Li-PE/C/Al(OH)$_3$ anode; the specific capacity values refer to the mass of the complete negative electrode, i.e., including the mass of the current collector in the case of Li-Cu and Li-PE/C/Al(OH)$_3$.

(11.63 mg cm^{-2}). Within the Li-Cu electrode, the bulky Cu current collector dominates the overall mass of the electrode, accounting for 77% of the total areal density, while it does not provide any additional capacity—in other words, it's largely "dead weight". Accordingly, the high mass and density of the current collector significantly compromises the total specific capacity of the lithium-

metal anode (in terms of the complete electrode including the current collector). When calculating the theoretical specific capacity of the neat Li, the Li-Cu, and the Li-PE/C/Al(OH)$_3$ electrode, it becomes evident that the Li-Cu electrode displays a relatively low theoretical specific capacity of 886 mAh g^{-1}, which is approximately one quarter of the theoretical specific capacity of metallic lithium with about 3860 mAh g^{-1} (Fig. 2c). Notably, when the very dense Cu is replaced with the less dense PE/C/Al(OH)$_3$ as current collector and mechanical support, the theoretical specific capacity of the Li-PE/C/Al(OH)$_3$ electrode increases to 2528 mAh g^{-1}. This is also reflected by the experimentally determined specific capacity values for the Li-PE/C/Al(OH)$_3$ electrode with 2237 mAh g^{-1}, which is close to the theoretical maximum and ca. thrice higher than the specific capacity of the Li-Cu electrode with 857 mAh g^{-1} (Fig. 2d–f).

3.2. Evaluation of the flame retardancy

To demonstrate the flame retardancy of PE/C/Al(OH)$_3$, we comparatively evaluated the flammability of the pure PE/C membrane, the PE/C membrane with 20 wt.% of Al(OH)$_3$, and the PE/C membrane with 40 wt.% of Al(OH)$_3$ (PE/C/Al(OH)$_3$). As shown in Fig. 3(a) and Video S1, the pure PE/C membrane burnt completely down in only 6 s after ignition. The addition of 20 wt.% Al(OH)$_3$ substantially slowed down the burning rate, taking more than 20 s after ignition (Fig. 3b and Video S2). Apparently, a concentration of 20 wt.% is not yet sufficient to fully prevent ignition of the polymer-based current collector. However, when adding 40 wt.% Al(OH)$_3$ to the PE/C membrane (PE/C/Al(OH)$_3$), the initial flame diminished within only 3 s and completely extinguished within 5 s (Fig. 3c), as the decomposition products covered the polymer

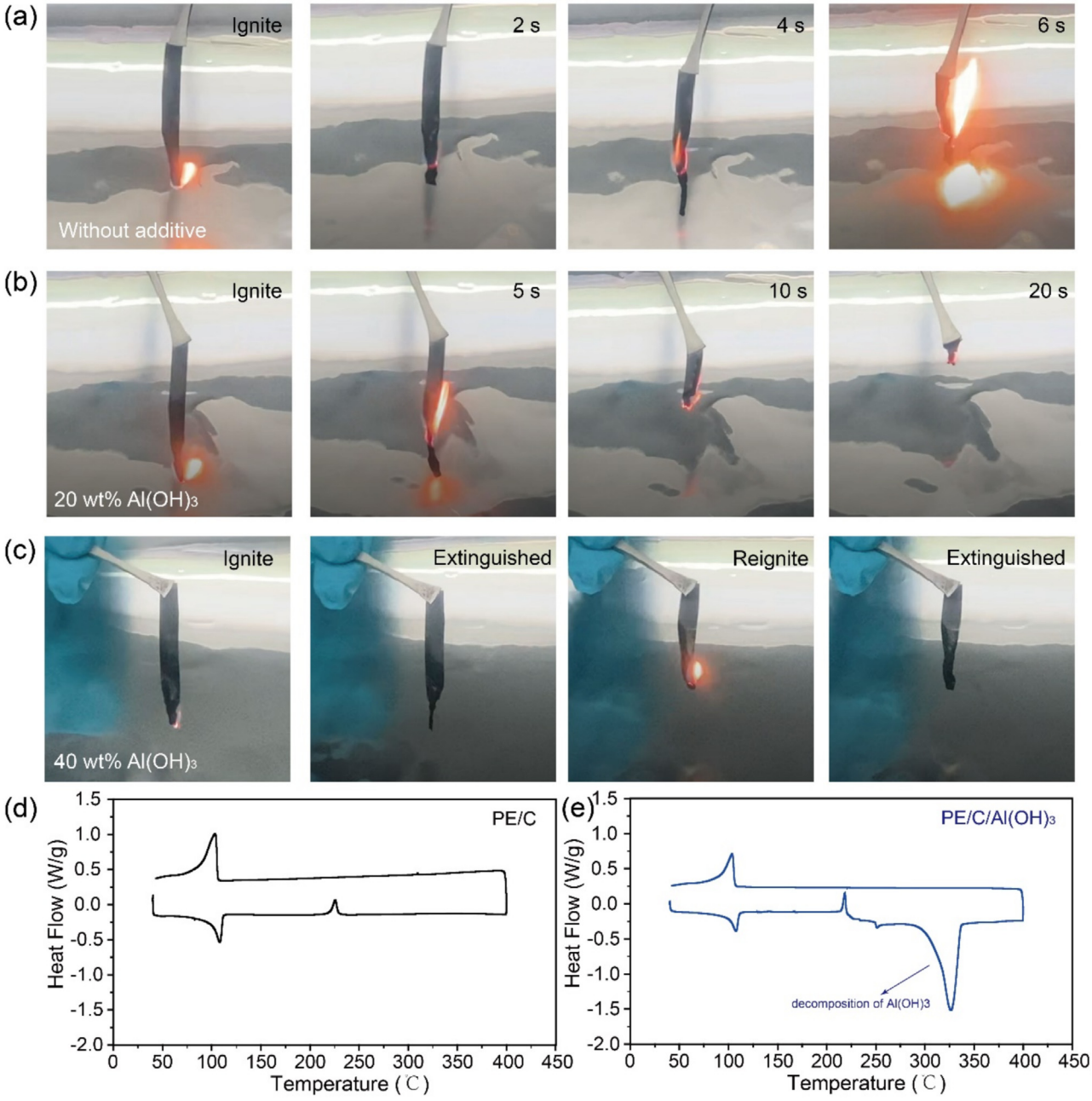

Fig. 3. Fire retardancy of the PE/C/Al(OH)$_3$ current collector and its single components. Photographs recording the flammability test of (a) the PE/C membrane, (b) the PE/C membrane with 20 wt.% Al(OH)$_3$, and (c) the PE/C membrane with 40 wt.% Al(OH)$_3$. DSC heat flow curve recorded for (d) the PE/C membrane and (e) the PE/C/Al(OH)$_3$ membrane (temperature range: 20 to 400 ℃, heating rate: 5 ℃ min^{-1} under the N_2 atmosphere).

surface, effectively isolating it from oxygen, and making it difficult to reignite again [31,32]. In fact, even though it was somehow possible to reignite the membrane, the flame quickly extinguished within only 2 s, underlining the exceptional flame retardancy properties of these membranes (Fig. 3c and Video S3).

To further investigate the flame retardancy of the PE/C/Al(OH)$_3$ current collector, differential scanning calorimetry (DSC) was performed (Fig. 3d, e). The heat flow curve of the neat PE/C membrane revealed a very reversible endothermic peak at approximately 115 °C, corresponding to the melting point of PE, and an exothermic peak at approximately 225 °C, attributed to the combustion of impurities on the C surface. The DSC traces recorded for the PE/C/Al(OH)$_3$ current collector show essentially the same features, except an additional endothermic peak at around 325 °C, indicative of the decomposition of Al(OH)$_3$, according to the following equation, as also evidenced by XRD (Fig. S5): Al(OH)$_3$ → Al(OOH) + H_2O.

This decomposition process and the evaporation of water consumes a significant amount of heat (as a matter of fact, the integration of the DSC data reveals an increase in heat absorption from about 660 to 1150 J g^{-1} when transitioning from PE/C to PE/C/Al(OH)$_3$), effectively mitigating the combustion of the polymer membrane. It appears noteworthy that, different from other flame retarding strategies, the Al(OH)$_3$ additive is sealed inside the polymer current collector so that it does not affect the electrochemical reactions during dis–/charge of the battery cell.

3.3. Morphology of the deposited lithium

Ex situ SEM and EDX were conducted to analyze the lithium deposition behavior on the Cu and PE/C/Al(OH)$_3$ current collectors in Li||Cu and Li||PE/C/Al(OH)$_3$ cells, as this has a crucial impact on the electrochemical performance. When 0.1 mAh cm^{-2} of lithium was deposited on the Cu current collector at a current density of 1 mA cm^{-2}, numerous long and slender lithium dendrites were observed randomly distributed over the Cu surface (Fig. 4a). Upon increasing the amount of lithium on the Cu to 1, 2, and 4 mAh cm^{-2}, the lithium deposition morphology was rather uneven with long and thin lithium dendrites. These are prone to dissolve/react to form "dead lithium", thereby leading to rapid capacity fading [33–35]. Additionally, lithium dendrites may penetrate the separator during battery cycling, resulting in short circuits and thermal runaway [36,37]. Moreover, even after plating 4 mAh cm^{-2} of lithium, the deposited layer did not completely cover the Cu current collector.

Differently, upon lithium deposition (0.1 mAh cm^{-2}) on the PE/C/Al(OH)$_3$ current collector, a rather compact layer of rather particle-like lithium deposits was observed on the surface of the PE/C/Al(OH)$_3$ membrane (Fig. 4b). Interestingly, even after 1 mAh cm^{-2} lithium deposition no slender lithium dendrites were detected at the anode. The formation of particle-like deposits instead of dendritic lithium deposits greatly reduces the risk of short circuits and is expected to increase the utilization of the metallic lithium. These results are further corroborated by conducting EDX mapping of the PE/C/Al(OH)$_3$ current collector following lithium plating, which revealed the formation of a homogeneous and compact deposition layer (Fig. 4d). The detected Al signal was rather low, indicating an essentially complete coverage of the current collector surface. Indeed, in sharp contrast to the Cu current collector, the lithium plated on PE/C/Al(OH)$_3$ and the presence of phosphorus as indicate SEI component showed greater

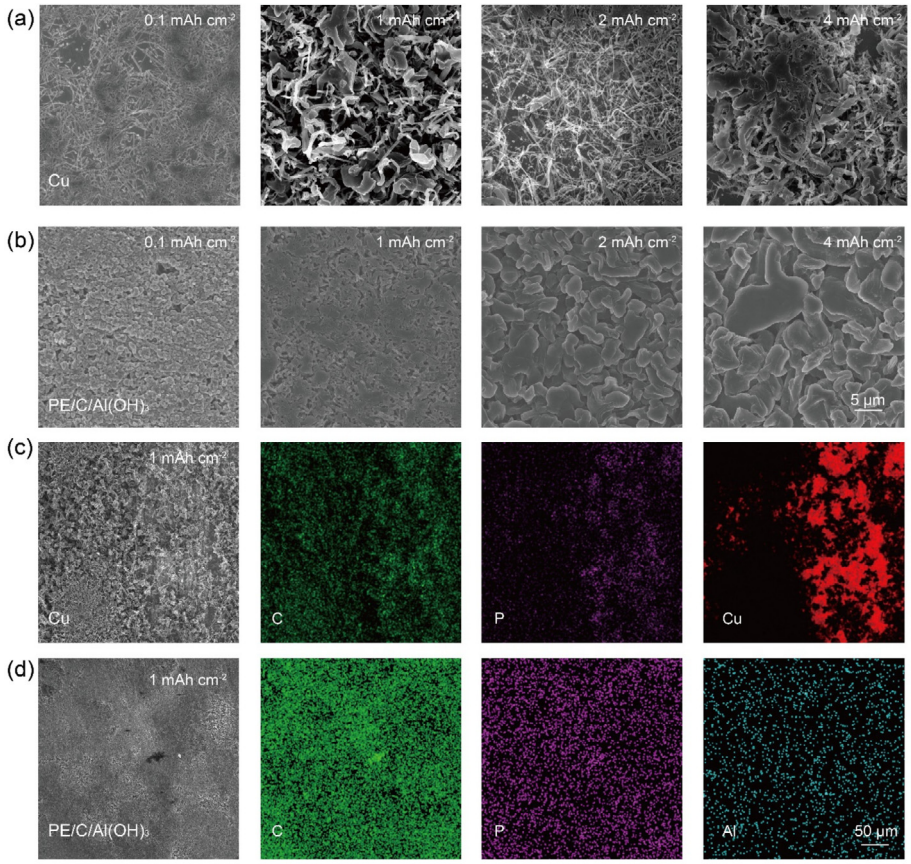

Fig. 4. Ex situ SEM/EDX analysis of the Cu and PE/C/Al(OH)$_3$ current collector after lithium plating. Top-view SEM micrographs of the (a) Cu surface and (b) PE/C/Al(OH)$_3$ surface after depositing 0.1, 1, 2, and 4 mA h cm^{-2} of lithium. SEM micrographs of the (c) Cu surface and (d) PE/C/Al(OH)$_3$ surface after depositing 1 mA h cm^{-2} of lithium and corresponding EDX mapping of C, P, Cu, and Al.

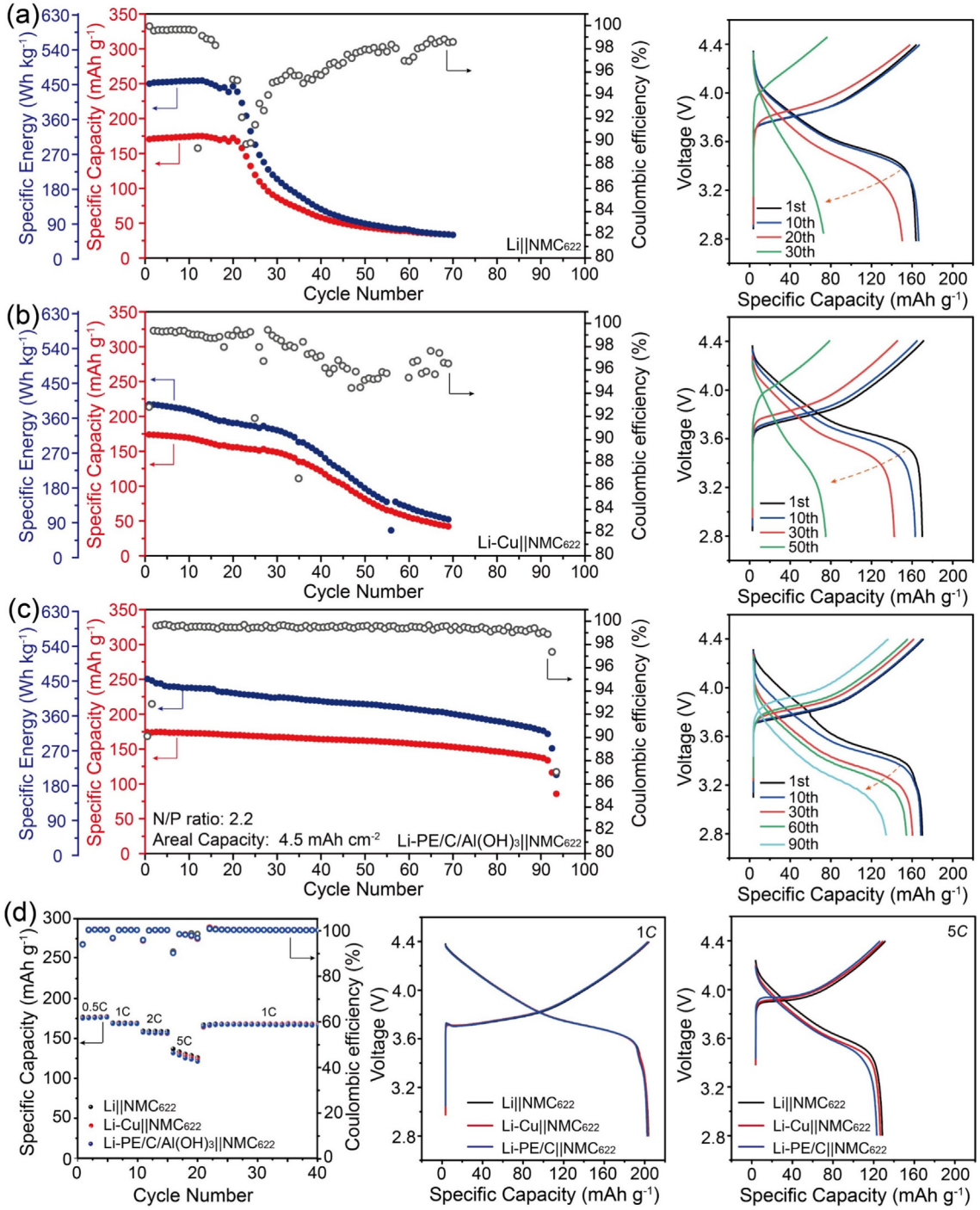

Fig. 5. Electrochemical performance of Li||NMC_{622} cells employing the different negative electrodes. Plot of the specific capacity, specific energy, and Coulombic efficiency vs. the cycle number (left) and selected dis-/charge profiles (right) recorded for the (a) Li||NMC_{622}, (b) Li-Cu||NMC_{622}, and (c) Li-PE/C/Al$(OH)_3$||NMC_{622} cells (active material mass loading of the NMC_{622} cathode: 25 mg cm^{-2}, charge/discharge rate: 0.3C/0.5C). (d) Rate capability (left) and the corresponding dis-/charge profiles at 1C (middle) and 5C (right); the active material mass loading of the NMC_{622} cathode was about 6.5 mg cm^{-2}.

uniformity, contributing to the improved cycling stability of the Li-PE/C/Al$(OH)_3$ anode (Fig. 4d). Apparently, the presence of Al$(OH)_3$ inside the membrane did not affect the homogeneity of the deposited lithium (see also Figs. S6 and S7 for lower resolution SEM micrographs). Furthermore, lithium deposition up to 2 and 4 mAh cm^{-2} resulted in the growth of relatively large particles rather than forming the irregular dendritic structures observed on the Cu surface. In line with these findings, the Tafel plot of the Li||PE/C/Al$(OH)_3$ cell showed a much lower current density (~0.68 mA cm^{-2}) than for the Li||Cu cell (3.41 mA cm^{-2}), which has been reported to result in the formation of larger and denser lithium deposits (Fig. S8) [38,39]. Such larger lithium particles possess a lower specific surface area, resulting in a reduced contact area with the electrolyte and, thus, decreased side-reactions, as also evidenced by an ex situ XPS analysis (Fig. S9), showing less electrolyte decomposition products on PE/C/Al$(OH)_3$ compared to Cu, which is beneficial for the cycling stability of LMB cells. In fact, the ex situ XPS analysis also reveals a superior reversibility of the

lithium stripping/plating process on PE/C/$Al(OH)_3$, indicated by the absence of any metallic lithium after stripping.

3.4. Evaluation in lithium-metal battery cells

The cycling performance of neat Li, Li-Cu, and Li-PE/C/$Al(OH)_3$ was evaluated in pouch cells with a thin (50 μm) lithium foil as the negative electrode and high mass loading NMC_{622} positive electrodes with an areal capacity of about 4.5 mA h cm^{-2}, resulting in an N/P ratio of ca. 2.2. Owing to the low thickness of the lithium foil, the Li||NMC_{622} cell delivered a very high specific energy of 454 Wh kg^{-1} based on the mass of both the cathode and anode, including the active material, conductive carbon, binder, and the current collector (Fig. 5a). Nonetheless, this high specific energy comes at the expense of a very limited cycling stability of the Li||NMC_{622} cell, with a rapid capacity fading after only 20 cycles. We have shown in a previous study that this fading is related to an extensive crack formation in the lithium foil owing to an uneven lithium deposition and stripping and, as a result, a loss of electronic contact [22].

The Li-Cu||NMC_{622} cell showed a similar specific capacity in the first cycle (174 mAh g^{-1}, based on the mass of NMC_{622}), but the specific energy of the Li-Cu||NMC_{622} cell was only 391 Wh kg^{-1}, i.e., about 14% lower than for the Li||NMC_{622} cell, due to the high mass and density of the Cu current collector (Fig. 5b; see Table S2 for the given mass input for the calculation of the specific energy). Nevertheless, the introduction of the Cu current collector significantly improved the cycling stability of the Li-Cu||NMC_{622} cell up to more than 30 cycles, before the capacity and Coulombic efficiency decreased more sharply. Despite this sacrifice in specific energy, the Li-Cu||NMC_{622} cell still provided a specific energy of around 263 Wh kg^{-1} in the 40th cycle, which is about 66% of its initial specific energy and significantly higher than the 27% (128 Wh kg^{-1}) energy retention of the Li||NMC_{622} cell. Apparently, the presence of an electron-conducting substrate is beneficial for the capacity retention and lithium utilization, despite potential corrosion effects at the metal | metal interface [40,41]; the latter effect might (amongst others) be responsible, in fact, for the slight fading right from the beginning—different from the Li||NMC_{622} cell—as apparent also from the continuous increase in overpotential (Fig. 5b right side).

The Li-PE/C/$Al(OH)_3$||NMC_{622} cell, eventually, provided a first cycle specific capacity of 173 mAh g^{-1}, i.e., essentially the same as for the other two cells, resulting in a specific energy of 449 Wh kg^{-1}, which is very close to the specific energy of the Li||NMC_{622} cell and almost 15% higher than the specific energy of the Li-Cu||NMC_{622} cell (Fig. 5c). Remarkably, the cycling stability was essentially tripled compared to the Li-Cu||NMC_{622} cell, with more than 90 cycles of stable cycling prior to cell fading. The capacity retention was almost 88% after 40 cycles, and more than 71% after 90 cycles. Apparently, the use of such a current collector helped to overcome the issue of a loss of electronic conductivity and, thus, accessibility of the lithium metal across the whole electrode, while avoiding any kind of corrosion issue and supporting a more homogeneous lithium deposition (see also Fig. 4) along with a high flexibility of the cell as such (see Fig. S10 for some bending and folding tests while powering an electronic device).

Fig. 5(d) displays the rate capability of the Li||NMC_{622}, Li-Cu||NMC_{622}, and Li-PE/C/$Al(OH)_3$||NMC_{622} cells. At a dis-/charge rate of 0.5C, all three cells exhibit the same specific capacity of 176 mAh g^{-1}. When the cells were subjected to a higher dis-/charge rate of 5C (5.5 mA cm^{-2}), the specific capacity of the Li-PE/C/$Al(OH)_3$||NMC_{622} cell still remained comparable to that of the Li||NMC_{622} and Li-Cu||NMC_{622} cells. This observation underscores the comparable rate capability of the Li-PE/C/$Al(OH)_3$ electrode to the Li and Li-Cu electrode, attributed to the sufficiently high electronic conductivity of the current collector in combination with the metallic lithium on top.

4. Conclusions

An ultralight, flame-retardant polymer-based current collector was designed that effectively enhances both the specific energy and safety of LMBs. Cells comprising an NMC_{622} positive electrode and a lithium-metal negative electrode employing such PE/C/Al$(OH)_3$ current collector provide a remarkable specific energy of 449 Wh kg^{-1} (taking into account the complete electrode), which represents an almost 15% increase compared to comparable cells employing a classic Cu current collector. In addition, these cells show an essentially tripled cycle life, benefiting from the homogenous lithium stripping/platting behavior on PE/C/$Al(OH)_3$ and the absence of a metal | metal interface. Finally, the flame-retardant additive $Al(OH)_3$, incorporated into the current collector, successfully suppresses the flammability of the polymer-based current collector, while remaining inactive during cycling. In sum, this approach leads to an enhanced performance and safety of LMBs, rendering this novel current collector design a potential alternative to classic metallic current collectors.

CRediT authorship contribution statement

Mintao Wan: Writing – original draft, Visualization, Methodology, Investigation, Formal analysis, Data curation, Conceptualization. **Huifang Fei:** Writing – review & editing, Investigation, Formal analysis, Data curation. **Haowen Liu:** Writing – review & editing, Investigation, Data curation. **Nae-Lih Wu:** Writing – review & editing, Supervision, Resources, Funding acquisition. **Stefano Passerini:** Writing – review & editing, Supervision, Resources, Methodology, Funding acquisition. **Dominic Bresser:** Writing – review & editing, Writing – original draft, Supervision, Resources, Methodology, Funding acquisition, Conceptualization.

Declaration of competing interest

The authors declare that they have no known competing financial interests or personal relationships that could have appeared to influence the work reported in this paper.

Acknowledgement

The authors would like to acknowledge financial support from the Helmholtz Association and the German Federal Ministry of Education and Research (BMBF) within the ExcellBattUlm project (03XP0257D) and the HighSafe-3 project (03XP0568A).

Appendix A. Supplementary material

Supplementary data to this article can be found online at https://doi.org/10.1016/j.jechem.2025.10.052.

References

[1] M.S. Whittingham, Chem. Rev. 114 (2014) 11414–11443.
[2] M. Armand, J.M. Tarascon, Nature 451 (2008) 652.
[3] M. Armand, P. Axmann, D. Bresser, M. Copley, K. Edström, C. Ekberg, D. Guyomard, B. Lestriez, P. Novák, M. Petranikova, W. Porcher, S. Trabesinger, M. Wohlfahrt-Mehrens, H. Zhang, J. Power Sources 479 (2020) 228708.
[4] W. Xu, J. Wang, F. Ding, X. Chen, E. Nasybutin, Y. Zhang, J.-G. Zhang, Energy Environ. Sci. 7 (2014) 513–537.
[5] J.M. Tarascon, M. Armand, Nature 414 (2001) 359–367.
[6] J. Liu, Z.N. Bao, Y. Cui, E.J. Dufek, J.B. Goodenough, P. Khalifah, Q.Y. Li, B.Y. Liaw, P. Liu, A. Manthiram, Y.S. Meng, V.R. Subramanian, M.F. Toney, V.V. Viswanathan, M.S. Whittingham, J. Xiao, W. Xu, J.H. Yang, X.Q. Yang, J.G. Zhang, Nat. Energy 4 (2019) 180–186.

[7] C. Niu, D. Liu, J.A. Lochala, C.S. Anderson, X. Cao, M.E. Gross, W. Xu, J.-G. Zhang, M.S. Whittingham, J. Xiao, J. Liu, Nat. Energy 6 (2021) 723–732.
[8] Y. Qiao, H. Deng, P. He, H.S. Zhou, Joule 4 (2020) 1445–1458.
[9] S. Kim, G. Park, S.J. Lee, S. Seo, K. Ryu, C.H. Kim, J.W. Choi, Adv. Mater. 35 (2023) 2206625.
[10] J. Xiao, Science 366 (2019) 426–427.
[11] Z. Wu, C. Wang, Z. Hui, H. Liu, S. Wang, S. Yu, X. Xing, J. Holoubek, Q. Miao, H.L. Xin, Nat. Energy 8 (2023) 340–350.
[12] P. Shi, X.B. Cheng, T. Li, R. Zhang, H. Liu, C. Yan, X.Q. Zhang, J.Q. Huang, Q. Zhang, Adv. Mater. 31 (2019) 1902785.
[13] C. Fang, J. Li, M. Zhang, Y. Zhang, F. Yang, J.Z. Lee, M.-H. Lee, J. Alvarado, M.A. Schroeder, Y. Yang, Nature 572 (2019) 511–515.
[14] P. Shi, Z.-Y. Liu, X.-Q. Zhang, X. Chen, N. Yao, J. Xie, C.-B. Jin, Y.-X. Zhan, G. Ye, J.-Q. Huang, Ifan E.L. Stephens, M.-M. Titirici, Q. Zhang, J. Energy Chem. 64 (2022) 172–178.
[15] W. Wu, W. Luo, Y. Huang, Chem. Soc. Rev. 52 (2023) 2553–2572.
[16] D. Li, Y. He, B. Chen, J. Xu, Q. Liu, S. Yang, W.-Y. Lai, Mater. Chem. Front. 8 (2024) 2727–2735.
[17] D. Li, J. Xu, Q. Liu, J. Cui, X. Han, S. Yang, W.-Y. Lai, Chem. Engineering J. 509 (2025) 161583.
[18] Y. Ye, L.-Y. Chou, Y. Liu, H. Wang, H.K. Lee, W. Huang, J. Wan, K. Liu, G. Zhou, Y. Yang, A. Yang, X. Xiao, X. Gao, D.T. Boyle, H. Chen, W. Zhang, S.C. Kim, Y. Cui, Nat. Energy 5 (2020) 786–793.
[19] Y.N. Chen, K. Fu, S.Z. Zhu, W. Luo, Y.B. Wang, Y.J. Li, E. Hitz, Y.G. Yao, J.Q. Dai, J.Y. Wan, V.A. Danner, T. Li, L.B. Hu, Nano Lett. 16 (2016) 3616–3623.
[20] M.M. Baig, S.A. Khan, H. Ahmad, J. Liang, G. Zhu, H. Pang, Y. Zhang, FlexMat 1 (2024) 79–99.
[21] H. Mao, S. Zhang, J. Liu, S. Wu, D. Liu, H. Li, L. Zhang, Y. Zhang, Q. Wu, T. Ma, FlexMat 1 (2024) 302–310.
[22] M. Wan, R. Gilles, J. Vacik, H. Liu, N.-L. Wu, S. Passerini, D. Bresser, Small 20 (2024) 2404437.
[23] J.H. Wang, Y. Yamada, K. Sodeyama, E. Watanabe, K. Takada, Y. Tateyama, A. Yamada, Nat. Energy 3 (2018) 22–29.
[24] L. Yu, J. Huang, S. Wang, L. Qi, S. Wang, C. Chen, Adv. Mater. 35 (2023) 2210789.
[25] Z. Chen, G.T. Kim, J.K. Kim, M. Zarrabeitia, M. Kuenzel, H.P. Liang, D. Geiger, U. Kaiser, S. Passerini, Adv. Energy Mater. 11 (2021) 2101339.
[26] P. Liang, H. Sun, C.L. Huang, G.Z. Zhu, H.C. Tai, J.C. Li, F.F. Wang, Y. Wang, C.J. Huang, S.K. Jiang, M.C. Lin, Y.Y. Li, B.J. Hwang, C.A. Wang, H.J. Dai, Adv. Mater. 34 (2022) 2207361.
[27] W.X. Ji, B.L. Jiang, F.X. Ai, H.X. Yang, X.P. Ai, RSC Adv. 5 (2015) 172–176.
[28] X.Y. Zhang, Q.W. Sun, C. Zhen, Y.H. Niu, Y.P. Han, G.F. Zeng, D.J. Chen, C. Feng, N. Chen, W.Q. Lv, W.D. He, Energy Storage Mater. 37 (2021) 628–647.
[29] T. Yim, M.-S. Park, S.-G. Woo, H.-K. Kwon, J.-K. Yoo, Y.S. Jung, K.J. Kim, J.-S. Yu, Y.-J. Kim, Nano Lett. 15 (2015) 5059–5067.
[30] Q. Xie, W. Li, A. Manthiram, Chem. Mater. 31 (2019) 938–946.
[31] A. Bunder, B. Japelj, B. Music, N. Rajnar, S. Gyergyek, R. Kostanjsek, P. Krajnc, Polym. Compos. 37 (2016) 1659–1666.
[32] J.H. Zhou, C. Zhang, C. Xie, H.M. Wang, H.N. Fan, Y.P. Guo, C. Wang, F. Chen, Y.C. Ding, Q.Y. Huang, Z.J. Zheng, Adv. Energy Mater. 14 (2023) 2303063.
[33] M. Tao, J. Chen, H. Lin, Y. Zhou, D. Zhao, P. Shan, Y. Jin, Y. Yang, J. Energy Chem. 96 (2024) 226–248.
[34] J. Wang, H. Hu, S. Duan, Q. Xiao, J. Zhang, H. Liu, Q. Kang, L. Jia, J. Yang, W. Xu, H. Fei, S. Cheng, L. Li, M. Liu, H. Lin, Y. Zhang, Adv. Funct. Mater. 32 (2022) 2110468.
[35] Q. Zhang, S. Liu, Y. Lu, L. Xing, W. Li, J. Energy Chem. 58 (2021) 198–206.
[36] X. Cheng, R. Zhang, C. Zhao, Q. Zhang, Chem. Rev. 117 (2017) 10403–10473.
[37] Y. Cheng, L. Jiang, X. Hu, Z. Yang, H. Xu, B. Kong, Y. Deng, L. Han, M. Zhang, X. Wei, Q. Wang, J. Energy Chem. 110 (2025) 311–335.
[38] Y.Y. Liu, X.Y. Xu, M. Sadd, O.O. Kapitanova, V.A. Krivchenko, J. Ban, J.L. Wang, X. X. Jiao, Z.X. Song, J.X. Song, S.Z. Xiong, A. Matic, Adv. Sci. 8 (2021) 2003301.
[39] J. Lopez, A. Pei, J.Y. Oh, G.J.N. Wang, Y. Cui, Z.A. Bao, J. Am. Chem. Soc. 140 (2018) 11735–11744.
[40] A. Kolesnikov, M. Kolek, J.F. Dohmann, F. Horsthemke, M. Börner, P. Bieker, M. Winter, M.C. Stan, Galvanic Adv. Energy Mater. 10 (2020) 2000017.
[41] J.F. Dohmann, F. Horsthemke, V. Küpers, S. Bloch, Y. Preibisch, A. Kolesnikov, M. Kolek, M.C. Stan, M. Winter, P. Bieker, Adv. Energy Mater. 11 (2021) 2101021.